BJRS

BRAZILIAN JOURNAL
OF
RADIATION SCIENCES
11-03 (2023) | 01-23 | e2300

Use of [^{18}F]FLT/PET for assessing the tumor evolution and monitoring the antitumor activity of rosmarinic acid in a mouse 4T1 breast tumor model

Pereira[a], J. M.; Schirmer[a], B. G. A.; Araujo[a], M. R.; Nascimento[a], L. T. C.; Ferreira[a], A. V.; Gonçalves[b], A. B. B.; Barcelos[c], L. S.; Cassali[b], G. D.; Silveira[a], M. B., Silva[a] J. B.; Malamut[a], C*

[a] *Centro de Desenvolvimento da Tecnologia Nuclear (CDTN), Unidade de Pesquisa e Produção de Radiofármacos, Av. Antônio Carlos 6.627, Campus da UFMG, Pampulha, 31270-901, Belo Horizonte, Minas Gerais, Brazil.*

[b]*Department of Physiology, Biological Science Institute, Universidade Federal de Minas Gerais, Belo Horizonte, Brazil.*

[c]*Department of General Patology, Biological Science Institute, Universidade Federal de Minas Gerais, Belo Horizonte, Brazil*

*malamut@cdtn.br.

ABSTRACT

The use of the tracer ^{18}F-fluoro-3'-deoxy-3'-L-fluorothymidine ([^{18}F]FLT) in positron emission tomography (PET) has been shown to be an effective tool for assessing tumor aggressiveness and early response to therapy. In this study, we investigated the applicability of [^{18}F]FLT/PET to study the antitumor and anti–lung metastatic effects of rosmarinic acid (RA) in highly invasive breast cancer. 4T1 mammary carcinoma cells were injected into the flank of female Balb/c mice. The animals were treated daily with RA until day 21 after the inoculation of tumor cells. [^{18}F]FLT/PET imaging was used to evaluate the response of primary tumors and lung metastases to RA treatment. PET Images showed a decreased [^{18}F]FLT uptake in the lungs of mice after RA treatment. The antitumor effect of RA appears to be related to the inhibition of cell migration, cell proliferation, and blood vessel formation in the primary tumor. Furthermore, the inflammatory response was modulated by RA, which reduced the accumulation of mast cells and neutrophils in the primary tumor and of macrophages in the lungs. In conclusion, [^{18}F]FLT/PET demonstrates the antitumor and antimetastatic effects of RA in a 4T1 breast tumor model. Furthermore, the findings suggest that RA modulates tumor angiogenesis and inflammation, resulting in antitumor and antimetastatic effects in a 4T1 breast carcinoma model.

Keywords: **[^{18}F]FLT/PET, rosmarinic acid, 4T1 mammary tumor, lung metastasis.**

ISSN: 2319-0612
DOI: https://doi.org/10.15392/2319-0612.2023.2300
Submitted: 2023-05-25
Accepted: 2023-09-15

1. INTRODUCTION

Breast cancer is highly prevalent and is the main cause cancer-related mortality among women worldwide [1]. Approximately 2.26 million cases of breast cancer were recorded in 2020, of which 685,000 deaths were noted, with almost two-thirds recorded in underdeveloped regions [2].

Breast cancer survival varies according to the stage at diagnosis. Metastasis, an advanced stage of cancer progression, is associated with increased morbidity and mortality [3]. For instance, in the United States, more than 18 million individuals are estimated to have a history of cancer [4], with an overall 5-year relative survival rate of 99% for local-stage disease, 85% for regional-stage disease, and 27% for distant-stage disease [5]. This indicates that the current treatment for metastatic breast cancer remains unsatisfactory. Therefore, the discovery of new therapies and antineoplastic drugs aimed at preventing tumor progression and metastasis is paramount in breast cancer therapy.

Positron emission tomography (PET) is an important tool for cancer detection and management. In breast cancer, this technique is used to detect metastases and monitor the treatment response [6]. Several types of tracers and radioisotopes have been developed to understand the tumor biology and its progression [7]. [^{18}F] fluorodeoxyglucose ([^{18}F]FDG) is currently the most widely used PET radiopharmaceutical in clinical oncology; however, its uptake is also detected in inflammatory cells and, hence, is not specific to tumor cells [7,8]. Studies have reported others radiopharmaceuticals that are more specific for clinical and preclinical applications, especially for cancer diagnosis, such as [^{18}F]-fluoro-3′-deoxy-3′- L-fluorothymidine ([^{18}F]FLT) [9,10].

[^{18}F]FLT is taken up by the cell via passive diffusion and Na^+-dependent carriers and is phosphorylated by thymidine kinase 1 (TK1) into [^{18}F]FLT-monophosphate, which is then trapped in the cells. TK1 is the principal enzyme involved in the salvage pathway of DNA synthesis [11], and its enzymatic activity is virtually absent in quiescent cells. However, in proliferating cells, it reaches a maximum during the late G1 and S phases of the cell cycle. Previous studies reported that TK1 activity is three to four times higher in malignant cells than in benign cells [12]. Thus, the radiopharmaceutical [^{18}F]FLT has been developed as a proliferation tracer. [^{18}F]FLT/PET imaging plays an important role in evaluating the response to cancer treatment and offers the possibility of differentiating between benign and malignant tissues as well as assessing the tumor aggressiveness and early response to therapy [13].

Rosmarinic acid (RA) is a natural phenolic ester compound found in plants of the Lamiaceae and Boraginaceae families, such as *Rosmarinus officinalis* [14]. This compound has been shown to exert antioxidant, anti-inflammatory, and antitumorigenic effects [15–17]. The anti-inflammatory activity of RA has been reported in both local and systemic inflammation models [18]. In addition, RA has been shown to exert antimetastatic effects in some cancer cell lineages, including colon, lung, and breast cancers [19]. However, the effect of RA treatment on 4T1 primary breast tumor evolution is unknown, and the mechanism by which RA inhibits the metastasis remains poorly elucidated. Thus, a more extensive investigation is crucial to determine the therapeutic efficacy of this compound.

Therefore, in this study, we aimed to evaluate the applicability of [^{18}F]FLT/PET for assessing the effects of RA on 4T1 mammary tumors, an animal model that closely mimics stage IV human breast cancer [20], by focusing on primary tumor evolution and lung metastatic commitment.

2. MATERIALS AND METHODS

2.1 Animals

All experiments were performed on adult female Balb/c mice aged 6–9 weeks and weighed 20–30 g. The mice were provided by the Animal Facility Center of the Federal University of Minas Gerais, Belo Horizonte, Brazil. The animals were kept in a temperature-controlled environment with 12/12-h dark–light cycles and had free access to water and food. Animal care protocols were performed in accordance with the guidelines of the National Council for the Control of Experiments on Animals (CONCEA). This study was approved by the CDTN Committee on Animal Experimentation (Protocol 01/2016).

2.2 4T1 murine mammary carcinoma murine model

The 4T1 murine mammary tumor cells (ATCC® CRL-2539™) were cultured in Dulbecco´s Modified Eagle's Medium (DMEM; Sigma-Aldrich, Switzerland), supplemented with 10% fetal bovine serum (FBS; Sigma-Aldrich, Switzerland) and 1% penicillin/streptomycin (Gibco by Life Technologies), in an incubator at 37 ºC and 5% CO_2 humidified atmosphere. An inoculum of 100 µl of DMEM containing 1×10^6 4T1 murine mammary carcinoma cells was injected into the left flank of Balb/c mice. The tumor diameter was measured twice per week up to day 21 following cell

inoculation, and the tumor volume was estimated using the following formula: tumor volume (mm^3) = (length × $width^2$)/2. We considered the length as the largest tumor diameter and the width as the perpendicular tumor diameter. The animals were sacrificed if ulcerations or discomfort occurred.

2.3 Rosmarinic acid treatment

The animals were randomly divided into two experimental groups: vehicle- and RA-treated. RA was dissolved in saline and administered orally (20 mg/kg/day). Saline was administered in the vehicle-treated group. RA was administered daily from day 5 after inoculating the tumor cells until the end of the experiment on day 21. The animals were weighed weekly to correct for the administered doses.

2.4 Evaluation of lung metastasis using MicroPET scan

The tracers [^{18}F]FLT and [^{18}F]FDG were obtained from the Nuclear Technology Development Center (CDTN, Belo Horizonte, Brazil). Quality control of [^{18}F]FLT included pH, chemical purity, radiochemical identity and purity, residual solvents, radionuclide identity and purity, bacterial endotoxins, and sterility tests, as previously reported [21].

Images of animals that received treatments 7, 14, and 21 days after 4T1 cell inoculation were acquired. Before the evaluation, the animals were fasted for a minimum of 4 h. For the analysis, 10.0-14.0 MBq of [^{18}F]FLT with a maximum volume of 100 µL were intravenously injected through the tail vein of the mice. After 60 min, the animals were anesthetized with 3.0–4.0% isoflurane in 100% oxygen and placed in a PET scanner (MicroPET - LabPET4 Solo, GE Healthcare Technologies). The same protocol was used for [^{18}F]FDG. The acquisition was performed for 15 min, corresponding to 5-bed positions. Radioactive decay of 18F was automatically corrected during the procedure. An image of the phantom was acquired and used to obtain a more precise factor for calibration purposes during the quantitative analysis performed in the next step. Radiopharmaceutical uptake in the lungs was assessed by calculating the maximum standard uptake value (SUVmax) in a given region of interest around the lungs. SUVmax is the most commonly used parameter for the highest uptake within a region of interest in the lungs. PMOD® software (version 3.3) was used for quantitative analysis.

2.5 Histological analysis

The mice were anesthetized and sacrificed through cervical dislocation 21 days after 4T1 cell inoculation. Samples of the primary tumor and lungs embedded in paraffin were sliced (5-µm thick), stained with hematoxylin and eosin, and examined using bright-field microscopy (Olympus BX41). Tumor angiogenesis was analyzed by counting the number of blood vessels in 10 fields (40× magnification) of the tumor, and the values were expressed as the number of vessels per field in each group. The metastatic commitment was analyzed by measuring the total metastatic area and calculating the percentage based on the total area of the lung sample. Analyses were performed using ImageJ software, version 1.48 (National Institutes of Health, USA).

To evaluate the presence of mast cells in the primary tumor and lungs, 5-µm thick slices of the samples were stained with toluidine blue (Neon Comercial, Brazil). Cell events were counted in five fields per slice (40× magnification), and the values were expressed as the mean of cell events per field in each group.

2.6 N-Acetyl-β-D-glucosaminidase and myeloperoxidase activity measurement

The effects of RA treatment on macrophage and neutrophil accumulation in the primary tumor and lungs were estimated by measuring myeloperoxidase (MPO) and N-Acetyl-β-D-glucosaminidase (NAG) enzyme activities as previously described [22]. Tumor and lung samples were collected on day 21 post-inoculation of 4T1 tumor cells and stored at -80 °C until the assays were performed.

2.7 Cell viability evaluation using trypan blue staining

To estimate the percentage of dead cells treated with different doses of RA, cell viability was evaluated using trypan blue staining as previously described [23,24]. Briefly, 3.5×10^4 4T1 cells were plated per well in a 24-well plate and cultured overnight. Next, the cells were treated with different concentrations of RA (50, 100, 200, and 400 µg/mL) diluted in DMEM with 0.5% FBS for 48 h. The control group was treated with the vehicle only. Finally, the floating and adhered cells (detached with trypsin solution) in each well were mixed and added to a solution containing 0.4% trypan blue (Sigma-Aldrich, Switzerland) at a concentration of 1:1. The number of trypan blue–positive dead cells and trypan blue–negative live cells were counted using a Neubauer chamber, visualized using an inverted phase contrast microscope (Zeiss Telaval 31) at 40× magnification.

The experiment was repeated three times with triplicates for each group per experiment. In all subsequent *in vitro* experiments, one nontoxic (viability similar to that of the vehicle control group) and one toxic concentration of RA were used.

2.8 Migration analysis using the gap closure assay

The migration capacity of 4T1 cells was evaluated using a scratch gap closure assay. First, 3×10^5 4T1 cells were plated per well in 24-well plates and cultured overnight to form monolayers. On the next day, a gap was made in the middle of the well using a sterile yellow tip and RA was added in desired concentrations (100 μg/mL and 200 μg/mL), diluted in DMEM supplemented with 0.5% FBS and hydroxyurea (Sigma-Aldrich, Switzerland) at 2 mM concentration to inhibit cell proliferation. Control groups were treated with the vehicle or DMEM supplemented with 10% FBS plus hydroxyurea at 2 mM concentration (positive control). Photographs of the gap areas were captured at 0 and 16 h after treatment. Areas without the cells were measured using Image Pro-Plus software (Media Cybernetics, USA). The percentage of gap closure was calculated as follows: Gap closure (%) = (Area without cells at 0 h - area without cells at 16 h)/ (Area without cells at 0 h) ×100. The experiment was repeated three times in duplicates for each group per experiment.

2.9 Evaluation of 4T1 tumor cell proliferation by analyzing 5-bromo-2'-deoxyuridine cell incorporation

The effect of RA on 4T1 tumor cell proliferation was evaluated by analyzing 5-bromo-2'-deoxyuridine cell incorporation (BrdU assay). Briefly, 3.5 $x10^3$ 4T1 cells were plated per well in a 96 wells plate and treated with 50 or 100 g/mL of RA diluted in DMEM with 0.5% FBS for 24h. The control group was treated with the vehicle only. The assay was performed using the Cell Proliferation ELISA BrdU Colorimetric kit (Roche Applied Science, Switzerland) following the manufacturer's instructions.

2.10 Statistical analysis

Statistical analyses were performed using GraphPad Prism 6.0 (Graphpad Software Inc., USA). Results are expressed as means ± standard deviation. Student´s t-tests were used to compare the two groups. *In vitro* results were subjected to one-way analysis of variance followed by Dunnett's post-hoc test. Statistical significance was set at $P < 0.05$.

3. RESULTS AND DISCUSSION

3.1 Use of [^{18}F]FLT and [^{18}F]FDG to assess tumor evolution in mouse 4T1 mammary tumor models and prediction of 4T1 breast cancer therapy response and lung metastasis

The tumor volume was evaluated weekly to track the tumor size, and the tumor volume curve was found to increase over time each week, as expected, in the [^{18}F]FLT and [^{18}F]FDG groups (Figures 1A and 1B). All PET image analyses were performed on the primary tumor and the lung, which is the first site of metastasis of 4T1 tumors and human breast cancer. The primary tumor showed a higher uptake of radiopharmaceuticals than the right hind limb muscle (Figures 1E and F). In addition, the graph shows an increase in [^{18}F]FDG uptake in the tumor on day 21 compared with that on day 14 ($P<0.05$). This increase in tumor uptake after 21 days could be attributed to a larger tumor volume and/or inflammation, as [^{18}F]FDG is taken up by both tumor and inflammatory cells [25]. The lungs also showed a higher uptake of [^{18}F]FDG than the right hind limb muscle on all three experimental days 7, 14, and 21 ($P<0.01$, $P<0.01$, and $P<0.05$, respectively). When the uptake of [^{18}F]FDG in the lungs was compared between the three experimental days, no statistically significant difference was observed (Figure 1C), indicating a similar uptake on days 7, 14, and 21.

Similar to the uptake of [^{18}F]FDG by the primary tumor cells, [^{18}F]FLT uptake in the animals increased compared with that at baseline (Figure 1F) on days 7, 14, and 21 ($P<0.01$, $P<0.05$, and $P<0.01$, respectively). These data demonstrate that [^{18}F]FLT, similar to [^{18}F]FDG, can be used to identify the primary tumor. However, [^{18}F]FLT uptake in the primary tumor decreased with time on day 14 compared with that on day 7 ($P<0.05$). This result reflects the specificity of [^{18}F]FLT, which was only detected at sites with a high cell proliferation index. According to Filho [26], most cells proliferate in the early phase of neoplasia development; however, as the tumor develops, the proportion of proliferative cells decreases. In addition, as the 4T1 tumor progressed, there was an influx of inflammatory cells and an increase in the number of necrotic cells [27]; these cell populations were not in the G1 or S phase of the cell cycle. The uptake of [^{18}F]FLT was lower after 21 days, but the difference was not statistically significant.

Interestingly, [^{18}F]FLT uptake was equivalent to the basal uptake in the lungs on day 7. This was not observed on later days (14 and 21), which presented a higher uptake in the lung than in the right lower limb muscle ($P<0.01$ and $P<0.05$, respectively; Figure 1D). In conclusion, these results indicate that basal [^{18}F]FLT uptake was observed in the lungs after 7 days, and, in the following

days after 14 and 21 days, this higher uptake could be associated with the development of lung metastases. Therefore, [^{18}F]FLT could be used to detect lung metastases. In addition, we observed a higher uptake of [^{18}F]FLT in the lungs on day 14 than on day 7 ($P<0.05$), supporting the idea that this uptake may be related to the development of metastases.

Figure 1: *Use of [^{18}F]FLT and [^{18}F]FDG PET tracer to access the tumor evolution in 4T1 murine mammary carcinoma models on days 7, 14, and 21 after the tumor inoculum.* **(A)** Growth curve of 4T1 after the tumor inoculum in the [^{18}F]FDG and **(B)** [^{18}F]FLT groups (n=5 animals in each group). **(C)** Uptake of [^{18}F]FDG and **(D)** [^{18}F]FLT in the lung. **(E)** Uptake of [^{18}F]FDG and **(F)** [^{18}F]FLT in the primary tumor (n=4 animals in each group). The right hind limb muscle is used as the control. Representative images obtained using microPET. The results are presented as means ± standard deviation *P<0.05 and **P<0.01, ***P<0.001 (Student's t-test). [^{18}F]FLT, [^{18}F]-fluoro-3′-deoxy-3′- L-fluorothymidine; [^{18}F] FDG, [^{18}F] fluorodeoxyglucose; PET, positron emission tomography.

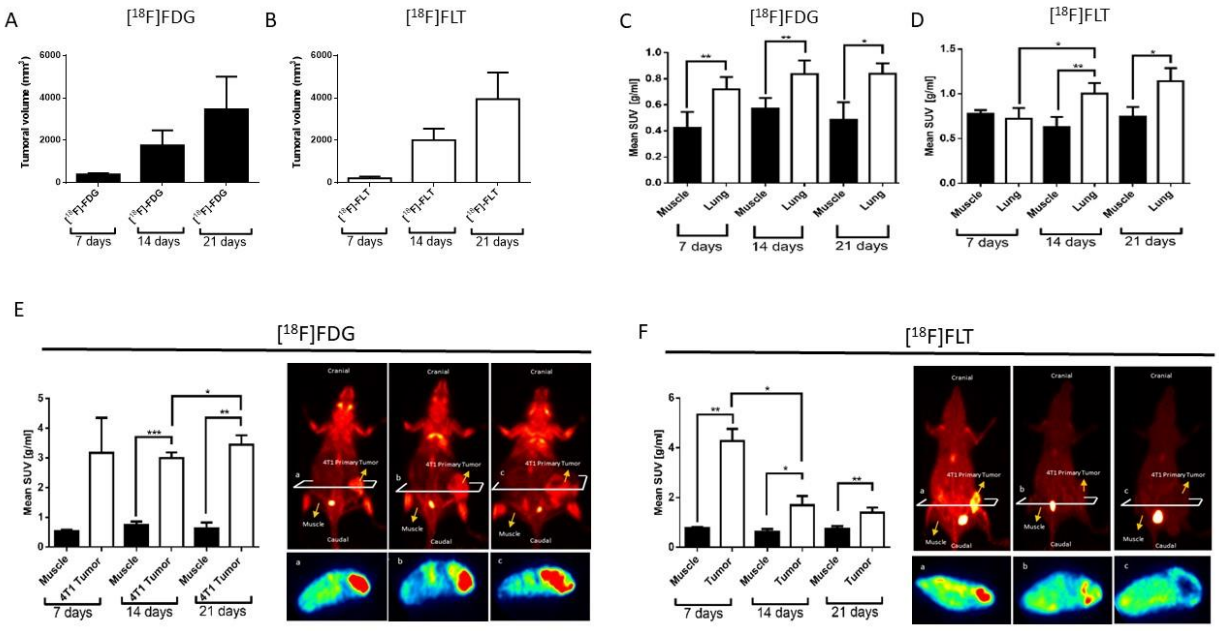

The effect of RA on metastasis in the lung was investigated using microPET, and the PET images showed a lower [^{18}F]FLT uptake in the lungs (Figure 2B) and primary tumor in the RA-treated group (Figure 2D). The lower uptake in the lungs on day 7 suggested a reduction in the metastasis in the first week after cell inoculation. By comparing the radiopharmaceuticals [^{18}F]FDG

and [^{18}F]FLT with respect to the antimetastatic effect of RA, we found that both tracers demonstrated a lower uptake in the lungs after treatment (Figures 3A and 3B). However, when only the uptake on day 21 was evaluated, we observed that only [^{18}F]FLT demonstrated a lower uptake in the lungs in the RA-treated group compared with that in the control group (Figure 3C).

Figure 2: *MicroPET of [^{18}F]FLT after RA treatment*. **(A)** Representative [^{18}F]FLT/PET images of saline- and **(B)** RA-treated mice. **(C)** [^{18}F]FLT uptake in the 4T1 primary mammary tumors of RA-treated mice (n=5) versus saline-treated mice (n=4). **(D)** [^{18}F]FLT uptake in the lungs of RA-treated mice (n=5) versus saline-treated mice (n=4). White arrows indicate the lung region and yellow arrows indicate the 4T1 primary mammary tumor on the left flank of the mice. The right hind limb muscle is used as the control. Representative images are obtained using microPET. The results are presented as means ± sem; *P<0.05 (Student's t-test). [^{18}F]FLT, [^{18}F]-fluoro-3′-deoxy-3′-L-fluorothymidine; [^{18}F] FDG, [^{18}F] fluorodeoxyglucose; PET, positron emission tomography; RA, rosmarinic acid.

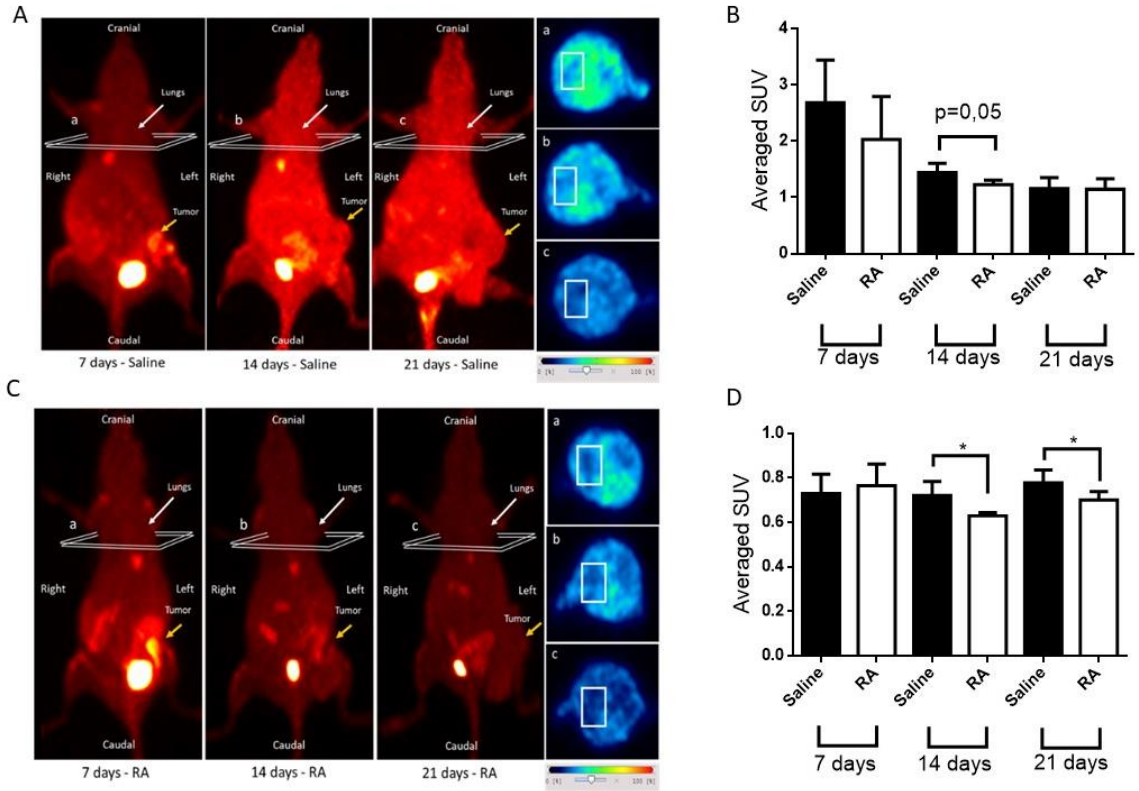

Figure 3: *Comparison between [^{18}F]FLT and [^{18}F]FDG uptake after RA treatment*. **(A)** Linear graph of [^{18}F]FDG and [^{18}F]FLT uptake in the lungs of treated and nontreated groups. **(B)** Quantification of the area under the curve of radiotracer uptake is shown in the line graph. **(C)** [^{18}F]FDG uptake in RA-treated mice versus saline-treated mice (n=4 animals per group) and [^{18}F]FLT uptake in RA-treated mice (n=5) versus saline-treated mice (n=4) on day 21. **(D)** Representative [^{18}F]FDG/PET images and **(E)** representative [^{18}F]FLT/PET images. The results are presented as means ± sem; * P<0.05 (Student's t-test). [^{18}F]FLT, [^{18}F]-fluoro-3′-deoxy-3′- L-fluorothymidine; [^{18}F] FDG, [^{18}F] fluorodeoxyglucose; PET, positron emission tomography; RA, rosmarinic acid.

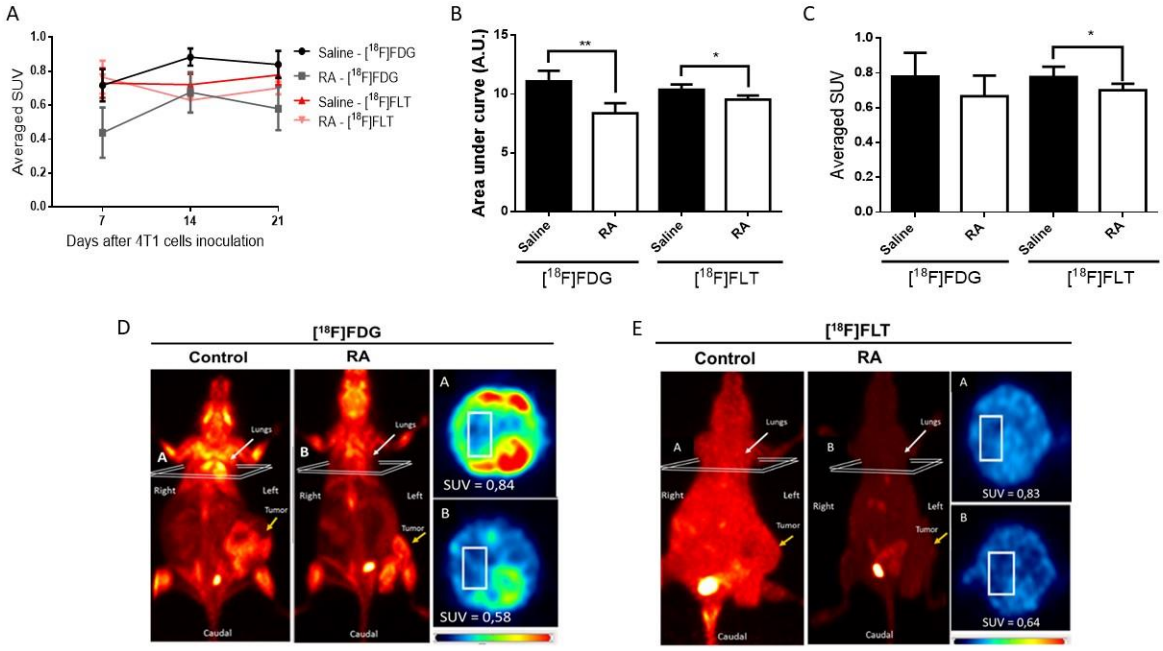

Although few studies have evaluated the use of [^{18}F]FLT in the diagnosis of breast tumors, there is still no consensus in the literature on the efficacy of this radiopharmaceutical. A few clinical trials have compared [^{18}F]FLT/PET and [^{18}F]FDG/PET uptake in patients with untreated breast cancer, and other studies have investigated the early responses to hormonal therapy, chemotherapy, and long-term survival in patients with breast cancer treated with neoadjuvant chemotherapy [10,28]. Mori et al. observed a strong correlation between [^{18}F]FLT/PET and [^{18}F]FDG/PET uptake in primary breast tumors and axillary lymph nodes [28]. Wesolowski et al. noted that a decrease in SUVmax on [^{18}F]FLT/PET scans during the first cycle of therapy can identify patients who are

likely to respond [29]. By contrast, Su et al. showed that the metabolic response assessed using preliminary [^{18}F]FLT/PET scans was not predictive of survival, whereas [^{18}F]FDG/PET scans provided better results in metastatic breast cancer [30]. Given the paucity of published studies and the conflicting data, the present study demonstrates the potential of [^{18}F]FLT/PET as a useful and effective tool for evaluating the presence of lung metastases and demonstrating the tumor-inhibitory effects of RA.

3.2 In vivo treatment with rosmarinic acid

The tumor volume and body weight of the animals were evaluated weekly to assess the evolution of the tumor and response to RA treatment, as shown in the representative image (Figure 4A). As expected, the tumor volume curve increased each week in all groups (Figure 4B). We observed that, 21 days after tumor inoculation, an RA dose of 20 mg/kg was effective in reducing tumor growth evolution. Measurement of the area under the curve (Figure 4C) showed a lower tumor growth rate in the RA-treated group ($P<0.03$).

Tumor angiogenesis was assessed by the histological analysis of primary tumor sections. The RA-treated group had a lower blood vessel density ($P=0.039$; Figure 4E), as shown in the representative images of each group in Figure 4D. In addition, histological analysis showed a significant reduction in the metastatic area only in the lungs of animals treated with 20 mg/kg of RA ($P=0.029$; Figure 4F), as illustrated in the representative images of each group in Figure 4G.

Figure 4: *Inhibition 4T1 tumor growth, angiogenesis, and lung metastasis by RA.* **(A)** Female Balb/c mouse on day 21 following 4T1 cell inoculation into the left flank. **(B)** Tumor volume is measured weekly following 4T1 cell inoculation. **(C)** Area under the curve of tumor volume kinetics. **(D)** Representative images of the histological analysis of the number of blood vessels in 4T1 mammary primary tumors after RA treatment. **(E)** Number of blood vessels per field in the histological sections in the RA-treated mice (n=5) versus saline-treated mice (n=4) on day 21. **(F)** Histological analysis of the lung metastasis area (% of the total area) in RA-treated mice (n=5) versus saline-treated mice (n=4) on day 21. **(G)** Representative images of lung metastases following RA treatment. Values are expressed as means ± sem; *P<0.05 and **P<0.01 compared with the control group. AU: arbitrary unit; RA, rosmarinic acid.

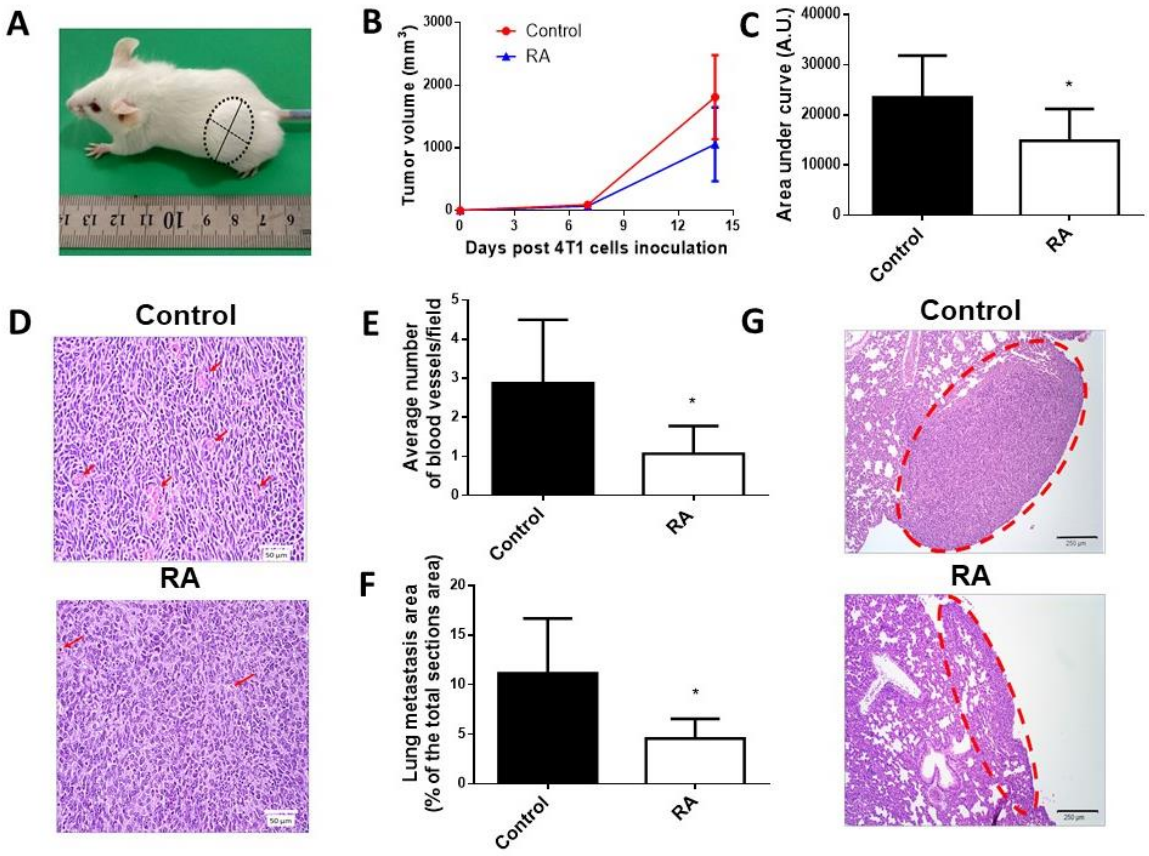

3.3 Rosmarinic acid effects on 4T1 tumor cell viability, cell proliferation, and cell migration *in vitro*

The effect of RA on the viability of 4T1 breast carcinoma cells was evaluated to exclude the possibility that the inhibitory effect of RA on these cells was caused by cytotoxicity *in vitro*. The viability of cells treated with 50 and 100 µg/ml of RA was similar to that of untreated cells, with a mortality rate of 25% after 48 h (Figure 5A), and the mortality rate of cells treated with 200 and 400 µg/mL reached 45% (P=0.08 and P=0.04, respectively). In subsequent *in vitro* experiments, RA doses of 100 and 200 µg/mL were used.

The 4T1 tumor cells treated with RA exhibited significantly lower BrdU incorporation than those treated with saline, indicating that RA at concentrations of 100 and 200 µg/mL significantly inhibited the proliferation of 4T1 cells (P=0.026 and P=0.0006, respectively; Figure 5B). Similarly, the migration capacity of 4T1 tumor cells was strongly inhibited by RA at concentrations of 100 and 200 µg/mL (P=0,04 and P= 0,012 respectively), as shown in Figures 5C and 5D.

Figure 5: *Impaired 4T1 mammary tumor cell viability, proliferation, and migration functions in vitro after RA treatment*. **(A)** Percentage of dead 4T1 tumor cells after 48 h of treatment with different doses of RA. Viability is analyzed by counting the number of cells in a Neubauer chamber after staining with trypan blue at 40× magnification. **(B)** Absorbance of BrdU incorporated into 4T1 tumor cells after 24 h of treatment with different doses of RA. The values derived from the three experiments are expressed as means ± sem, with duplicates in each group. **(C)** Representative images of the gap closure capacity of 4T1 cells after 24 h of treatment with different doses of RA. **(D)** Percentage of closure from the initial gap area. All values derived from the three experiments are expressed as means ± sem, with duplicates of each group. *P<0.05 and *P<0.01 compared with the control group. AU: arbitrary unit; RA, rosmarinic acid; BrdU, 5-bromo-2'-deoxyuridine.

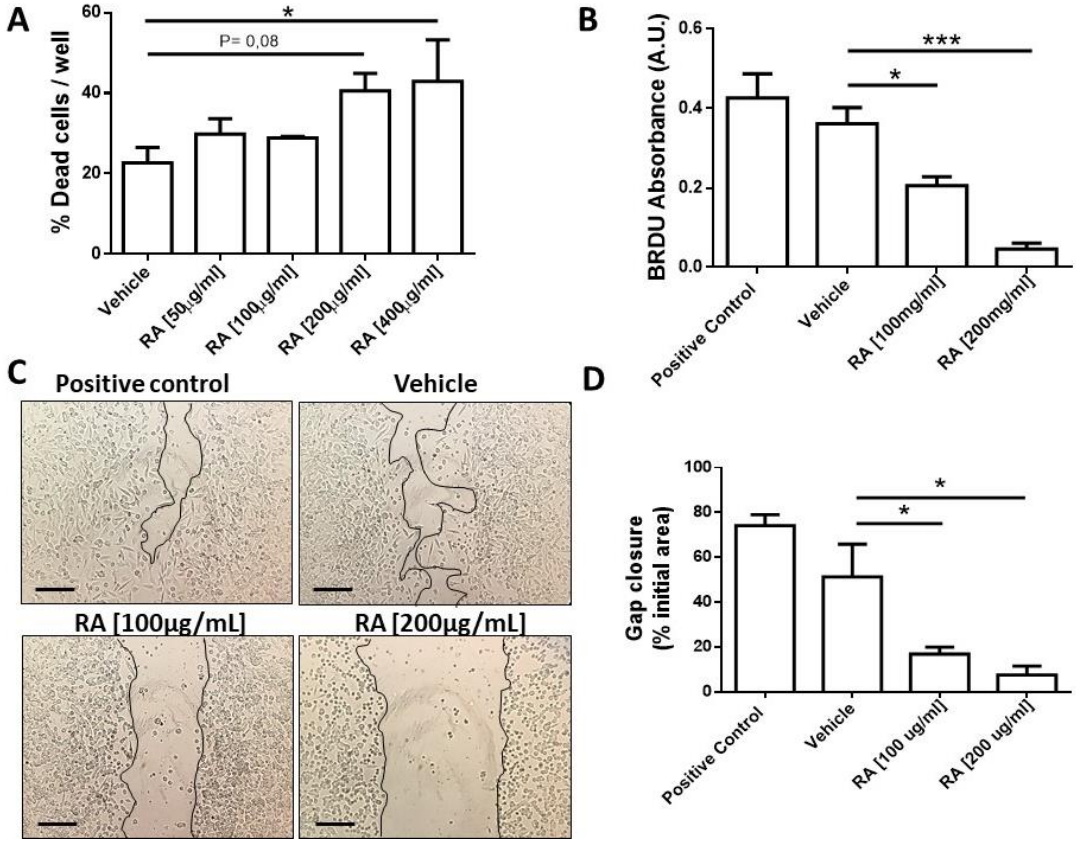

3.4 Modulation of inflammatory response by rosmarinic acid

MPO activity, but not NAG activity, was reduced in the primary tumors of RA-treated mice, indicating reduced local accumulation of neutrophils (P=0.029 and A, respectively; Figure 6C). In the lungs, NAG activity was reduced in RA-treated mice (P=0.033; Figure 6B), indicating a lower

number of macrophages in the lung tissue. However, MPO activity increased in mice treated with RA in the lungs (P=0.008; Figure 6D), indicating increased neutrophil accumulation in the lungs of these animals.

Histological analysis after toluidine blue staining showed a lower density of mast cells in the tumors of treated mice than in those in the control group (P=0.005; Figure 6E and G); however, no significant differences were observed in the lungs (P=0.06; Figures 5F and H).

Figure 6: *RA modulates inflammatory cell infiltration in the primary tumor and lungs*. **(A)** NAG and **(C)** MPO levels in the primary tumor of mice in the saline- and RA-treated groups. **(B)** NAG and **(D)** MPO levels in the lungs of mice in the saline- and RA-treated groups, expressed as optical density (OD) per 100 mg of tissue. **(E)** Mean number of mast cells per field in the tumor and **(F)** lung tissue slices. **(G)** Representative images of the primary tumor and **(H)** lungs collected 21 days following 4T1 cell inoculation from animals in the saline- and RA-treated groups. The scale bar corresponds to 50 µm. The values are presented as means ± sem. *P<0.05 and **P<0.01 compared with the control group. RA, rosmarinic acid; NAG, N-Acetyl-β-D-glucosaminidase; MPO, myeloperoxidase.

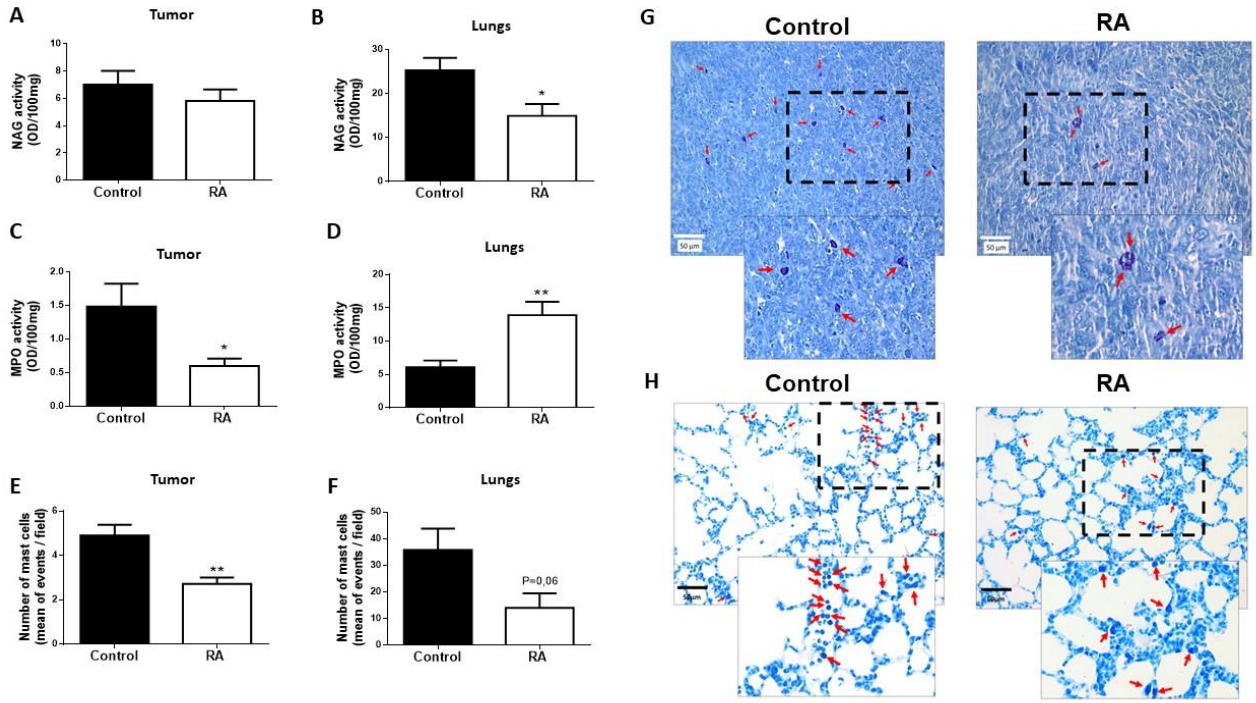

Several anticancer agents have been discovered by screening natural products or plants. RA, a polyphenol found in plants, such as *Rosmarinus officinalis*, has shown potent and effective antitumor effects against various cancers [16,31,32]. In the present study, we demonstrated that RA exerts antitumor and antimetastatic effects in the 4T1 breast carcinoma model and elucidated the mechanism of these effects.

In clinical trials, changes in the tumor volume after treatment is often used as an alternative marker of survival, and tumor size reduction is associated with a good response to cancer treatment [33]. Interestingly, a previous study by our group showed that RA treatment reduced the volume of 4T1 breast tumors [34]. In the present study, we confirmed this finding and showed that RA effectively inhibited tumor development. Furthermore, the body weight of the animals in this study was lower, probably because of the observed reduction in the tumor volume.

It is well-known that the formation of new blood vessels is crucial for tumor growth [35]. In this study, we observed a reduced number of blood vessels in the primary tumor of animals treated with RA, concomitant with slower tumor growth. This finding suggests that the antitumor effect of RA is partly attributed to the inhibition of tumor angiogenesis. Moreover, increased density of mast cells has previously been associated with increased angiogenesis in canine mammary tumors [36]. Remarkably, we found a lower number of mast cells in 4T1 primary tumors of RA-treated mice, suggesting an association. In addition, we observed a trend toward lower mast-cell density in the lungs of these animals.

Breast cancer cells are capable of colonizing several different organs, with the lungs, bone, liver, and pleura being the most common [37]. The mouse 4T1 breast tumor model closely resembles human stage IV breast cancer and is capable of metastasizing from the primary tumor to the liver, lungs, bone, and brain via a hematogenous pathway [20]. Xu et al. [31] previously showed that RA can inhibit bone metastasis in bone-seeking breast cancer cells. In the present study, we investigated the effects of RA on the development of lung metastases. Breast cancer has previously been associated with increased glucose consumption and can, therefore, be visualized using the glucose analog [^{18}F]FDG through PET imaging [38]. Interestingly, we observed a lower [^{18}F]-FDG uptake in the lungs of RA-treated mice, suggesting a lower number of 4T1 metastatic cells in the organ. Consistent with this finding, histological analysis showed that RA treatment reduced the area of metastatic involvement in the lungs.

Previous studies have shown that rosemary extract reduces breast cancer cell proliferation [39] and decreases cell viability when treated with conventional chemotherapeutic agents [40]. Similarly, treatment with RA resulted in decreased cell viability of breast cancer lines MCF -7 and MDA-MB -231BO [31,41] and sensitization of a resistant cell line to the chemotherapeutic agent [42]. In the present study, we found that RA decreased the viability of 4T1 cells *in vitro* and inhibited their proliferation and migration. These functions are essential for tumor development and metastasis. Therefore, we hypothesized that RA treatment may reduce tumor growth and lung metastasis *in vivo* by directly inhibiting 4T1 cell survival, proliferation, and motility.

The inflammatory response plays a critical role in tumor growth and metastasis. Inflammation influences every step in tumor development, including tumorigenesis, angiogenesis, invasion, and metastasis [43]. Interestingly, some of the anticarcinogenic effects of RA were shown to be because of the suppression of the secretion of angiogenic and inflammatory factors [16]. In the present study, we demonstrated that RA can modulate the accumulation of inflammatory cells in 4T1 primary tumors and the lungs of mice. Macrophages and neutrophils have been shown to play important roles in the development of breast tumors. Macrophages contribute to breast tumorigenesis through the secretion of growth factors, such as tumor cell proliferation, invasiveness, angiogenesis, and metastasis [44]. Indeed, a higher density of macrophages with proangiogenic and protumorigenic phenotypes in the tumor stroma has been shown to correlate with a poor prognosis in breast cancer [45]. Similarly, neutrophils in primary tumors can stimulate tumor angiogenesis, suppress the immune response, and release protumorigenic factors [46]. Moreover, neutrophils have been shown to play an important role in promoting metastasis in various breast tumor models [47]. Interestingly, the data of the present study suggest a lower accumulation of neutrophils in the 4T1 primary tumors of mice treated with RA, although no difference in the presence of macrophages was detected between the groups. However, in the lungs, treatment with RA decreased NAG activity, indicating reduced accumulation of macrophages in the tissue, consistent with the reduced metastasis observed in the histological analysis.

Interestingly, RA treatment increased the accumulation of neutrophils in the lungs of mice in the present study. Previous studies have described the accumulation of neutrophils in premetastatic lungs in various breast cancer models, and their numbers have been shown to increase during metastatic progression [47]. Therefore, RA may exacerbate this response. However, as previous studies have shown that neutrophils support metastasis, and, in the present study, RA reduced the

metastatic growth, we hypothesized that RA has a greater effect on the survival, proliferation, and migratory capacity of 4T1 tumor cells, which affect the development of lung metastases. However, further studies are needed to confirm these hypotheses.

This study demonstrates that RA inhibits the development of 4T1 mouse breast tumors and the formation of lung metastases by inhibiting tumor angiogenesis. Moreover, the results strongly suggest an important role for the anti-inflammatory effect of RA in inhibiting the growth of 4T1 mammary tumors and lung metastases. In addition, RA has an inhibitory effect on the proliferation and migration of 4T1 tumor cells. These results provide new insights into the antitumor mechanisms of RA and suggest that RA is a potential therapeutic agent for the development of drugs against highly invasive stage IV breast cancer.

4. CONCLUSION

In conclusion, the overall results indicate that the radiopharmaceuticals [^{18}F]FDG and [^{18}F]FLT are useful for monitoring the development of primary breast tumors. In addition, [^{18}F]FLT appears to be more specific than [^{18}F]FDG in identifying lung metastases. These data suggest that [^{18}F]FLT is more efficient for assessing tumor development and identifying metastases in mouse models of 4T1 breast cancer. Interestingly, [^{18}F]FLT/PET demonstrated the antitumor effect of RA after treatment. *In vivo* and *in vitro* experiments demonstrated that RA inhibited the development of 4T1 mouse breast tumors and the formation of lung metastases by inhibiting tumor angiogenesis. These results strongly suggest an important role of the anti-inflammatory effect of RA in the growth inhibition of 4T1 mammary tumors and lung metastases. Moreover, RA inhibited the proliferation and migration of 4T1 tumor cells. We conclude that [^{18}F]FLT/PET is a useful tool for the early prediction of metastasis and the treatment effect of RA.

ACKNOWLEDGMENT

We thank Dr. Pollyana Castro and Lorena de Assis for providing technical support, the staff of the Radiopharmaceutical Research and Production Unit, and the Molecular Imaging Laboratory of CDTN/CNEN.

REFERENCES

[1] LUO, C.; LI, N.; LU, B.; CAI, J.; LU, M.; ZHANG, Y.; et al. Global and regional trends in incidence and mortality of female breast cancer and associated factors at national level in 2000 to 2019. **Chin Med J (Engl),** v. 135, p. 42–51, 2022.

[2] WILKINSON, L.; GATHANI, T. Understanding breast cancer as a global health concern. **Br J Radiol,** v. 95, 2022.

[3] GIAQUINTO, A.N.; SUNG, H.; MILLER, K.D.; KRAMER, J.L.; NEWMAN, L.A.; MINIHAN, A.; et al. Breast Cancer Statistics, 2022. **CA Cancer J Clin,** v. 72, p. 524–541, 2022.

[4] GALLICCHIO, L.; DEVASIA, T.P.; TONOREZOS, E.; MOLLICA, M.A.; MARIOTTO, A. Estimation of the Number of Individuals Living With Metastatic Cancer in the United States. **JNCI J Natl Cancer Inst,** v. 114, p. 1476–1483, 2022.

[5] HOWLADER, N.; NOONE, A.M.; KRAPCHO, M.; MILLER, D.; BISHOP, K.; KOSARY, C.L.; YU, M.; RUHL, J.; TATALOVICH, Z.; MARIOTTO, A.; LEWIS, D.R.; CHEN, H.S.; FEUER, E.J.C.K (eds). SEER Cancer Statistics Review, 1975-2014. **National Cancer Institute**, Bethesda, MD, https://seer.cancer.gov/csr/1975_2014/, based on November 2016 SEER data submission, posted to the SEER web site, April 2017.

[6] PAYDARY, K.; SERAJ, S.M.; ZADEH, M.Z.; EMAMZADEHFARD, S; SHAMCHI, S.P.; GHOLAMI, S.; et al. The Evolving Role of FDG-PET/CT in the Diagnosis, Staging, and Treatment of Breast Cancer. **Mol Imaging Biol**, v. 21, p. 1–10, 2019.

[7] HADEBE, B.; HARRY, L.; EBRAHIM, T.; PILLAY, V.; VORSTER, M. The Role of PET/CT in Breast Cancer. **Diagnostics,** v. 13, p. 597, 2023.

[8] MING, Y.; WU, N.; QIAN, T.; LI, X.; WAN, D.Q.; LI, C.; et al. Progress and Future Trends in PET/CT and PET/MRI Molecular Imaging Approaches for Breast Cancer. **Front Oncol,** v.10, 2020.

[9] CRIȘAN, G.; MOLDOVEAN-CIOROIANU, N.S.; TIMARU, D-G.; ANDRIEȘ, G.; CAINAP, C.; CHIȘ, V. Radiopharmaceuticals for PET and SPECT Imaging: A Literature Review over the Last Decade. **Int J Mol Sci,** v. 23, p. 5023, 2022.

[10] ROMINE, P.E.; PETERSON, L.M.; KURLAND, B.F.; BYRD, D.W.; NOVAKOVA-JIRESOVA, A.; MUZI, M.; et al. 18F-fluorodeoxyglucose (FDG) PET or 18F-fluorothymidine (FLT) PET to assess early response to aromatase inhibitors (AI) in women with ER+ operable breast cancer in a window-of-opportunity study. **Breast Cancer Res**, v. 23, p. 88, 2021.

[11] XU, W.; YU, S.; XIN, J.; GUO, Q. 18F-FLT and 18F-FDG PET-CT imaging in the evaluation of early therapeutic effects of chemotherapy on Walker 256 tumor-bearing rats. **Exp Ther Med**, v.12, p. 4154–4158, 2016.

[12] ALWADANI B, DALL'ANGELO S, FLEMING IN. Clinical value of 3'-deoxy-3'-[18F]fluorothymidine-positron emission tomography for diagnosis, staging and assessing therapy response in lung cancer. **Insights Imaging**, v. 12, p. 90, 2021.

[13] HISHAR, H.; PRICE, R.; FATHINUL, F.; AHMAD, S.; EDIE, L.; WING, F.; ASSUNTA, C.; NORDIN, A.J. Potential of 3'-fluoro-3' deoxythymidine as a cellular proliferation marker in PET oncology examination. **Pertanika J Sci Technol,** v. 24, p. 41–52, 2016.

[14] PETERSEN, M.; SIMMONDS, M.S.J. Rosmarinic acid. **Phytochemistry**, v. 62, p. 121–125, 2003.

[15] ADOMAKO-BONSU, A.G.; CHAN, S.L.; PRATTEN, M.; FRY, J.R. Antioxidant activity of rosmarinic acid and its principal metabolites in chemical and cellular systems: Importance of physico-chemical characteristics. **Toxicol In Vitro**, v. 40, p. 248–255, 2017.

[16] CAO, W.; HU, C.; WU, L.; XU, L.; JIANG, W. Rosmarinic acid inhibits inflammation and angiogenesis of hepatocellular carcinoma by suppression of NF-κB signaling in H22 tumor-bearing mice. **J Pharmacol Sci. Elsevier Ltd**, v. 132, p. 131–137, 2016.

[17] YOOU, M.; PARK, C.L.; KIM, M-H.; KIM, H-M.; JEONG, H-J. Inhibition of MDM2 expression by rosmarinic acid in TSLP-stimulated mast cell. **Eur J Pharmacol,** v.771, p. 191–198, 2016.

[18] ROCHA, J; EDUARDO-FIGUEIRA, M.; BARATEIRO, A.; FERNANDES, A.; BRITES, D.; BRONZE, R.; et al. Anti-inflammatory Effect of Rosmarinic Acid and an Extract of Rosmarinus officinalis in Rat Models of Local and Systemic Inflammation. **Basic Clin Pharmacol Toxicol,** v.116, p. 398–413, 2015.

[19] HAN, Y-H.; KEE, J-Y.; HONG, S-H. Rosmarinic Acid Activates AMPK to Inhibit Metastasis of Colorectal Cancer. **Front Pharmacol,** v. 9, p. 68, 2018.

[20] PULASKI, B. A.; OSTRAND-ROSENBERG, S. Mouse 4T1 breast tumor model. **Curr Protoc Immunol.** Chapter 20: Unit 20.2. 2001.

[21] NASCIMENTO, L.T.C.; SILVEIRA, M.B.; FERREIRA, S.M.Z.M.D.; SILVA, J.B. Comparison between Two Ethanolic Solutions for 3'-Deoxy-3'-[^{18}F]Fluorothymidine Elution. **Adv Chem Eng Sci,** v. 07, p. 23–33, 2017.

[22] CASSINI-VIEIRA, P.; MOREIRA, C.; DA SILVA, M.; BARCELOS, L.S. Estimation of Wound Tissue Neutrophil and Macrophage Accumulation by Measuring Myeloperoxidase (MPO) and N-Acetyl-β-D-glucosaminidase (NAG) Activities. **BIO-PROTOCOL,** v. 5, 2015.

[23] FURTADO, R.A.; DE ARAUJO, F.R.R.; RESENDE, F.A.; CUNHA, W.R.; TAVARES, D.C. Protective effect of rosmarinic acid on V79 cells evaluated by the micronucleus and comet assays. **J Appl Toxicol**, v. 30, p. 254–259, 2010.

[24] ZHANG, L.; MIZUMOTO, K.; SATO, N.; OGAWA, T.; KUSUMOTO, M.; NIIYAMA, H.; et al. Quantitative determination of apoptotic death in cultured human pancreatic cancer cells by propidium iodide and digitonin. **Cancer Lett.** v.142, p. 129–137, 1999.

[25] BAKHEET, S.M.B.; POWE, J.; KANDIL, A.; EZZAT, A.; ROSTOM, A.; AMARTEY, J. F-18 FDG Uptake in Breast Infection and Inflammation. **Clin Nucl Med,** v. 25, p. 100, 2000.

[26] FILHO, G.B. **Bogliolo - Patologia Geral**, 4th ed., Rio de Janeiro: Guanabara Koogan; 2009. p. 233-282.

[27] TAO, K.; FANG, M.; ALROY, J.; SAHAGIAN, G.G. Imagable 4T1 model for the study of late stage breast cancer. **BMC Cancer,** v. 8, p. 228, 2008.

[28] MORI. M.; FUJIOKA, T.; ICHIKAWA, R.; INOMATA, R.; KATSUTA, L.; YASHIMA, Y.; et al. Comparison of 18F-fluorothymidine Positron Emission Tomography/Computed Tomography and 18F-fluorodeoxyglucose Positron Emission Tomography/Computed Tomography in Patients with Breast Cancer. **Tomography,** v. 8, p. 2533–2546, 2022.

[29] WESOLOWSKI, R.; STOVER, D.G.; LUSTBERG, M.B.; SHOBEN, A.; ZHAO, M.; MROZEK, E.; et al. Phase I Study of Veliparib on an Intermittent and Continuous Schedule in Combination with Carboplatin in Metastatic Breast Cancer: A Safety and [18F]-Fluorothymidine Positron Emission Tomography Biomarker Study. **Oncologist,** v. 25, p. e1158–e1169, 2020.

[30] SU, T-P.; HUANG, J-S.; CHANG, P-H.; LUI, K-W.; HSIEH, JC-H.; NG, S-H.; et al. Prospective comparison of early interim 18F-FDG-PET with 18F-FLT-PET for predicting treatment response and survival in metastatic breast cancer. **BMC Cancer,** v. 21, p. 908, 2021.

[31] XU, Y.; JIANG, Z.; JI, G.; LIU, J. Inhibition of bone metastasis from breast carcinoma by rosmarinic acid. **Planta Med,** v. 76, p. 956–962, 2010.

[32] XU, Y.; XU, G.; LIU, L.; XU, D.; LIU, J. Anti-invasion effect of rosmarinic acid via the extracellular signal-regulated kinase and oxidation-reduction pathway in Ls174-T cells. **J Cell Biochem,** v. 111, p. 370–9, 2010.

[33] JENSEN, M.M.; KJAER, A. Monitoring of anti-cancer treatment with (18)F-FDG and (18)F-FLT PET: a comprehensive review of pre-clinical studies. **Am J Nucl Med Mol Imaging**, v. 5, p. 431–456, 2015.

[34] DE ALMEIDA SCHIRMER BG, DE ARAUJO MR, SILVEIRA MB, PEREIRA JM, VIEIRA LC, ALVES CG, et al. Comparison of [18F]Fluorocholine and [18F]Fluordesoxyglucose for assessment of progression, lung metastasis detection and therapy response in murine 4T1 breast tumor model. **Appl Radiat Isot**, v. 140, p. 278–288, 2018.

[35] LANDSKRON G, DE LA FUENTE M, THUWAJIT P, THUWAJIT C, HERMOSO MA. Chronic inflammation and cytokines in the tumor microenvironment. **J Immunol Res**, v. 2014, p. 149185, 2014.

[36] LAVALLE G., BERTAGNOLLI A., TAVARES WL., FERREIRA MAN., CASSALI G. Mast cells and angiogenesis in canine mammary tumor. **Arq Bras Med Veterinária e Zootec**, v. 62, p. 1348–1351, 2010.

[37] SONI A, REN Z, HAMEED O, CHANDA D, MORGAN CJ, SIEGAL GP, et al. Breast Cancer Subtypes Predispose the Site of Distant Metastases. **Am J Clin Pathol,** v. 143, p. 471–478, 2015.

[38] BUCK AK, SCHIRRMEISTER H, MATTFELDT T, RESKE SN. Biological characterisation of breast cancer by means of PET. **Eur J Nucl Med Mol Imaging**, v. 31 Suppl 1, p. S80-7, 2004.

[39] ĐILAS S, KNEZ Ž, ČETOJEVIC-SIMIN D, TUMBAS V, ŠKERGET M, ČANADANOVIC-BRUNET J, et al. In vitro antioxidant and antiproliferative activity of three rosemary (Rosmarinus officinalis L.) extract formulations. **Int J Food Sci Technol**, v. 47, p. 2052–2062, 2012.

[40] GONZALEZ-VALLINAS M, REGLERO G, RAMIREZ DE MOLINA A. Rosemary (Rosmarinus officinalis L.) Extract as a Potential Complementary Agent in Anticancer Therapy. **Nutrition and Cancer**, p. 1221–1229, 2015.

[41] YESIL-CELIKTAS, O.; SEVIMLI, C.; BEDIR, E.; VARDAR-SUKAN, F. Inhibitory effects of rosemary extracts, carnosic acid and rosmarinic acid on the growth of various human cancer cell lines. **Plant Foods Hum Nutr**, v. 65, p. 158–163, 2010.

[42] BERDOWSKA, I.; ZIELINSKI, B.; FECKA, I.; KULBACKA, J.; SACZKO, J.; GAMIAN A. Cytotoxic impact of phenolics from Lamiaceae species on human breast cancer cells. **Food Chem**, v. 141, p. 1313–1321, 2013.

[43] GALUN, E. Liver inflammation and cancer: The role of tissue microenvironment in generating the tumor-promoting niche (TPN) in the development of hepatocellular carcinoma. **Hepatology**, v. 63, p. 354–356, 2016.

[44] TARIQ, M.; ZHANG, J.; LIANG, G.; DING, L.; HE, Q.; YANG, B. Macrophage Polarization: Anti-Cancer Strategies to Target Tumor-Associated Macrophage in Breast Cancer. **J Cell Biochem**, v. 118, p. 2484–2501, 2017.

[45] HOLLMEN, M.; KARAMAN, S.; SCHWAGER, S.; LISIBACH, A.; CHRISTIANSEN, A.J.; MAKSIMOW, M.; et al. G-CSF regulates macrophage phenotype and associates with poor overall survival in human triple-negative breast cancer. **Oncoimmunology**, v. 5, p. e1115177, 2016.

[46] YOUN, J-I.; NAGARAJ, S.; COLLAZO, M.; GABRILOVICH, D.I. Subsets of myeloid-derived suppressor cells in tumor-bearing mice. **J Immunol**, v. 181, p. 5791–802, 2008.

[47] WCULEK, S.K.; MALANCHI, I. Neutrophils support lung colonization of metastasis-initiating breast cancer cells. **Nature**, v. 528, p. 413–417, 2015.